High Efficiency Immobilization of Sulfur on Nitrogen-Enriched Mesoporous Carbons for Li–S Batteries

Fugen Sun, Jitong Wang, Huichao Chen, Wencheng Li, Wenming Qiao, Donghui Long,* and Licheng Ling

State Key Laboratory of Chemical Engineering, East China University of Science and Technology, Shanghai, China

S *Supporting Information*

ABSTRACT: Nitrogen-enriched mesoporous carbons with tunable nitrogen content and similar mesoporous structures have been prepared by a facile colloid silica nanocasting to house sulfur for lithium–sulfur batteries. The results give unequivocal proof that nitrogen doping could assist mesoporous carbon to suppress the shuttling phenomenon, possibly via an enhanced surface interaction between the basic nitrogen functionalities and polysulfide species. However, nitrogen doping only within an appropriate level can improve the electronic conductivity of the carbon matrix. Thus, the dependence of total electrochemical performance on the nitrogen content is nonmonotone. At an optimal nitrogen content of 8.1 wt %, the carbon/sulfur composites deliver a highest reversible discharge capacity of 758 mA h g^{-1} at a 0.2 C rate and 620 mA h g^{-1} at a 1 C rate after 100 cycles. Furthermore, with the assistance of PPy/PEG hybrid coating, the composites could further increase the reversible capacity to 891 mA h g^{-1} after 100 cycles. These encouraging results suggest nitrogen doping and surface coating of the carbon hosts are good strategies to improve the performance carbon/sulfur-based cathodes for lithium–sulfur batteries.

KEYWORDS: *lithium–sulfur battery, nitrogen-enriched mesoporous carbon, sulfur cathode, sulfur–carbon composite, surface coating*
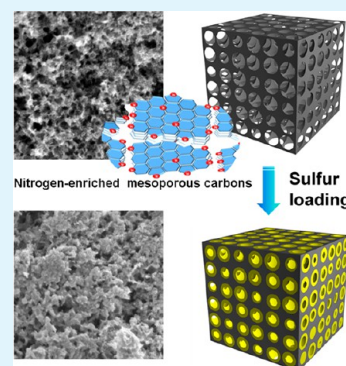
INTRODUCTION

Lithium–sulfur (Li–S) batteries are considered to be a promising energy-storage solution for the increasing demand for higher energy/power density.[1,2] Sulfur cathodes offer an order of magnitude higher capacity (theoretical capacity 1675 mA h g^{-1}) at an operating voltage of 2.1 V (vs Li/Li$^+$).[3] While the high capacity can significantly enhance the energy density of the batteries, the lower operating voltage can also offer better safety. Moreover, utilization of sulfur is advantageous because of its low cost and nontoxicity.[4] It is not, therefore, surprising that this system keeps the attention of battery developers for several decades. However, a commercially viable Li–S battery has not yet been really realized due to the following problems that remained unsolved: (i) poor cycle life and high self-discharge due to the dissolution of the polysulfide intermediates and (ii) low utilization and limited rate capability of sulfur cathodes due to the insulating nature of sulfur and the discharge product.[5,6]

Recently, significant advances have been achieved via using conductive carbon materials as hosts for immobilizing sulfur, to partly overcome the above-mentioned drawbacks in Li–S batteries.[7,8] Generally, the conductive carbon framework constrains the sulfur within its channels and generates essential electrical contact. Meanwhile the sorption properties of the porous carbon could trap the intermediate polysulfides and suppress the shuttle phenomenon.[9–11] It is further reported that the characteristics of the carbon hosts, such as pore size,[12] porosity,[13,14] and morphology[15] are also critically important to ensure efficient confinement of the sulfur. Moreover, polymer modification of the carbon surface could further improve the utilization of sulfur, which provides a chemical gradient to retard diffusion of the polysulfides into the electrolyte.[16] With help of these strategies, polysulfide dissolution into electrolyte could be prohibited to a certain degree, and in turn, the effective utilization of sulfur and the cycling stability are remarkably improved.

The properties of carbon materials as hosts not only depend on the textural characteristics but also on the surface chemistry and electrical conductivity. Generally, the heteroatomic dopant modifies the surface chemistry and electronic structures of the carbon hosts.[17] Among various dopants (phosphorus,[18] sulfur,[19] boron,[20] nitrogen[21]), nitrogen is most attractive which could substantially improve the carbon wettability, basic property, adsorptive ability, surface polar, and conductivity.[22] Recently, Sun et al.[23] first reported that the Li–S cathode based on nitrogen-doped mesoporous carbon/sulfur composites exhibited improved electrochemical performance compared with activated carbon/sulfur cathode. They concluded that nitrogen-doping could enhance activity toward sulfur reduction, providing higher discharge potential and initial capacity, but both cathodes still showed considerable capacity fading with cycling due to the polysulfide shuttling. Unfortunately, this work used two kinds of carbon hosts with completely different porous structures (micropore vs meso-

pore) and different sulfur loadings (24 vs 41 wt %). Thus it is hard to discern whether the porosity or the nitrogen doping or both of them play a role in the improved electrochemical performance of the carbon/sulfur cathodes. In addition, the nitrogen doping was achieved by high temperature NH_3 treatment, with only a limited surface doping (3.3 wt % from XPS results). Such a low nitrogen doping level does not change the properties of the bulk carbon as much.[17]

In contrast, in situ doping of carbons using nitrogen containing precursors can realize a homogeneous incorporation of nitrogen into the carbon material with a controlled chemistry, which could greatly modify the properties of the corresponding bulk carbon structure.[24] Here we prepared a series of mesoporous carbons via a simple colloidal silica nanocasting method using melamine, phenol, and formaldehyde as precursors. The obtained carbons had very similar mesoporous structures but a controllable nitrogen doping level. This could thus minimize the influence of the porosity, which could prompt us to focus on tracing the effects of nitrogen doping on the performance of the mesoporous carbon/sulfur cathodes. The electrochemical performance was found to be strongly dependent on the nitrogen doping level. Our experiments gave an unequivocal proof that only an appropriate content of nitrogen doping could improve the electronic conductivity and immobilize the sulfur and polysulfides, resulting in the superior sulfur utilization and cycle life of the sulfur composites. Furthermore, we explored the unique surface coating of PPy/PEG based hybrid polymer for further improving the electrode performance. With the assistance of PPy/PEG hybrid coating, considerable increase in delivered discharge capacity was achieved. These encouraging results suggest that tailoring surface chemistry and surface coating of the carbon hosts are good strategies to improve the electrochemical performance of carbon/sulfur-based cathodes for Li−S batteries.

■ EXPERIMENTAL SECTION

Preparation of the Nitrogen-Enriched Mesoporous Carbons. The nitrogen-enriched mesoporous carbons (NMC) were synthesized via a colloidal silica assisted sol−gel process, using phenol, melamine, and formaldehyde as the carbon precursor, similar to our previous report.[25] In a typical synthetic procedure, 3.67 g phenol (39 mmol) and 6.33 g formaldehyde (37 wt %, 78 mmol) were dissolved in 50 mL of 0.2 M NaOH solution (10 mmol). The mixture was stirred at 70 °C for 40 min. Then, 4.92 g melamine (39 mmol) and 9.50 g formaldehyde (107 mmol) were added to the above solution to react for 30 min with consecutive agitation until the solution became clear. Next, 50 g Ludox SM-30 sol (30 wt % SiO_2) was added to the above solution under stirring. The mixture was transferred to a sealed bottle and heated at 80 °C for 3 days. The obtained hydrogels were directly dried at 80 °C in an ambient condition, followed by the carbonization at 800 °C for 3 h with a heating rate of 5 °C min^{-1} in a nitrogen flow. The NMCs were obtained by dissolution of the silica nanoparticles in 2 M NaOH solution at 80 °C, isolated by filtration, washed with distilled water until the pH did not change, and dried at 100 °C. In this work, four samples with different nitrogen contents were prepared, which were denoted as M/P-x, where x represents the mole ratio of melamine to phenol. The total polymer concentration was fixed at 15 g/100 mL, while the colloidal silica was used as 15 g/100 mL for nitrogen-containing samples and 21 g/100 mL for the nitrogen-free M/P-0 sample.

Preparation of the NMC/S Composites. The NMC/S composites were prepared following a conventional melt-diffusion strategy.[26] The sublimed sulfur and as-prepared NMCs with various weight ratios were mixed homogeneously. The mixture was degassed in a vessel and then sealed under vacuum. The melt infiltration was further carried out in the vacuum-sealed vessel at 155 °C for 10 h. Then, the temperature was increased to 300 °C for 2 h to vaporize the superfluous sulfur on the outer surface of carbon diffusing entirely into the pores. The as-prepared NMCs/S composites were denoted as NMC/S-x, where x wt % represents the sulfur content.

Preparation of the Polypyrrole/Polyethyleneglycol-Coated NMC/S Composites. Polypyrrole/Polyethyleneglycol (PPy/PEG) coating was achieved by dispersing the M/P-1/S-60 in a solution containing PEG1000 and pyrrole monomer, followed by an in situ chemical oxidative polymerization.[27]

Typically, 0.33 g purified pyrrole monomer, 0.01 g PEG1000, and 1.5 g as-prepared NMC/S composites were placed in a 50 mL round-bottom flask. A 0.7 g portion of $FeCl_3$·$6H_2O$ as the oxidation agent was dispersed in 25 mL hydrochloric acid (0.1 mol L^{-1} HCl).[28] The resulting solution was added to the flask. The reaction was allowed to proceed for 12 h. During this time, the mixture was kept at ∼4 °C and stirred vigorously. The resulting PPy/PEG-coated NMC/S composites were recovered by filtration, washed with water and acetone, and dried in an oven (∼60 °C) until a constant weight was reached.

Material Characterization. Elemental analysis was carried out using Elemental Vario EL III. The carbon (C), hydrogen (H), and nitrogen (N) contents of the carbons were determined directly using the thermal conductivity detector.

The surface chemistry of the samples was analyzed using an Axis Ultra DLD X-ray photoelectron spectroscopy. The X-ray source operated at 15 kV and 10 mA. The working pressure was lower than 2 × 10^{-8} Torr (1 Torr = 133.3 Pa). The C_{1s}, N_{1s} XPS spectra were measured at 0.1 eV step size. The N_{1s} XPS signals were fitted with mixed Lorentzian−Gaussian curves, and a Shirley function was used to subtract the background using a XPS peak processing software.

Raman spectra were recorded with a Renishaw system 1000 with an argon-ion laser operating at 514 nm with a charged-coupling-device detector.

Power electrical resistivity measurements were carried out at room temperature using the four-contact method. The samples were filled in a Teflon cylinder with inner diameter of 16 mm, and two stainless-steel plungers were used to deliver 4 MPa pressure through a hydraulic press device. The current and voltage through the two stainless-steel plungers were recorded using two Keithley 2000 digital multimeters.

The thermogravimetric analysis (TA Instrument Q600 Analyzer) was carried out at a nitrogen flow rate of 100 mL min^{-1}. The samples were heated to 800 °C with a rate of 10 °C min^{-1}.

The morphologies of samples were observed under scanning electron microscopy (SEM, JEOL 7100F) and transmission electron microscopy (TEM, JEOL 2100F). The SEM mapping was observed under scanning electron microscopy (SEM, FEI Q-300).

Nitrogen adsorption/desorption isotherms were measured at 77 K with a Quadrasorb SI analyzer. Before the measurements, the NMC were degassed in vacuum at 473 K for 12 h while the C/S composites were degassed at 333 K for at least 12 h. The Brunauer−Emmett−Teller (BET) method was utilized to calculate the specific surface area. The total pore volume was calculated using a single point at relative pressure of 0.985. The pore size distributions were derived from desorption branch by using the Barrett−Joyner−Halenda (BJH) model.

Electrochemical Tests. The NMC/S cathode materials were slurry-cast onto aluminum current collectors. Typically, 80 wt % of the NMC/S composite, 10 wt % carbon black (Super P Conductive Carbon Black), and 10 wt % PVDF were mixed with N-methyl-2-pyrrolidone (NMP). The slurries were coated on aluminum current collectors and dried at 60 °C overnight. Electrochemical tests of these electrode materials were performed using coin cells with the sulfur composite cathode and lithium metal as the counter electrode. The electrolyte was 1 M bis(trifluoromethane) sulfonimide lithium salt (LiTFSI) dissolved in a mixture of 1.3-dioxolane (DOL) and dimethoxymethane (DME) (1:1 by volume). The separator was a microporous membrane (Celgard 2400). The cell was assembled in an argon filled glovebox. The galvanostatic charge−discharge test and cyclic voltammetry measurements (CV) were conducted using an Arbin battery cycler (Arbin, BT2000, USA). All capacity values were

5631

dx.doi.org/10.1021/am400958x | ACS Appl. Mater. Interfaces 2013, 5, 5630−5638

calculated on the basis of sulfur mass. Electrochemical impedance spectroscopy (EIS) was performed with an electrochemical working station PCI4/300 (Gamry Instrument, Warminster, PA, USA). The sinusoidal excitation voltage applied to the coin cells was 5 mV, with frequency range from 100 kHz to 0.01 Hz. All the electrochemical tests were performed at room temperature.

■ RESULTS AND DISCUSSION

Characterization of the NMCs. The NMCs with tunable nitrogen content and developed mesoporous structure were prepared on the basis of a conventional colloidal silica nanocasting process, using phenol−melamine−formaldehyde polymer as carbon precursor and commercial silica sol as template. Keys to the successful synthesis of the NMCs lie in the incorporation of high-nitrogen-content melamine into phenolic precursors that can inherit nitrogen atoms into carbon framework under pyrolysis conditions. Moreover, the synthesis is very flexible for tailoring their chemical nature only by changing the initial melamine/phenol (M/P) mole ratio in the precursors. As shown in Table 1, elemental analysis discloses

Table 1. Chemical Nature, Pore Parameters, and Electrical Resistivity of the NMCs

| samples | element analysis | | XPS | | $S_{BET}{}^a$ m^2 g^{-1} | $V_T{}^b$ cm^3 g^{-1} | ρ^c Ω cm |
	N wt %	N/C at/at	N at %	N/C at/at			
M/P-0	0	0	0	0	693	2.2	12.7
M/P-0.5	4.3	0.04	12.5	0.18	777	2.4	2.3
M/P-1	8.1	0.08	20.4	0.31	731	2.6	6.4
M/P-2	11.9	0.13	24.5	0.40	770	2.4	23.6

^{a}BET specific surface area. ^{b}Total pore volume (P/P_0 = 0.985). ^{c}Electrical resistivity measured using a four-contact method under the pressure of 4 MPa.

that the nitrogen content can be controlled in a wide range from 0 to 12 wt %. Increasing M/P ratio can apparently increase the nitrogen content. Highest nitrogen content is achieved as 11.9 wt % for M/P-2 precursors. More detailed elemental compositions are given in Supporting Information Table S1.

The XPS survey spectra of the NMCs possess three peaks centered at 284.6, 400.0, and 513.4 eV, corresponding to C_{1s}, N_{1s}, and O_{1s}, respectively, thus excluding the presence of any other impurities (Figure 1a). The surface N/C ratios of the NMCs from XPS results are also given in Table 1 and Supporting Information Table S2, which are almost three times higher than those from elemental analysis. This can be explained by the surface specificity of XPS measurements, suggesting nitrogen atoms are apt to gather in the surface rather than the bulk of carbon framework. The XPS spectra of C_{1s} (Supporting Information Figure S1) show a very similar asymmetric peak shape. The main peak at 284.6 eV is related to the graphitic carbon, indicating that most of the C atoms are arranged in conjugated honeycomb lattices. The N_{1s} spectra (Figure 1b) are curve-fitted into three peaks with binding energies of 398.5 ± 0.3, 400.5 ± 0.3, and 401.6 ± 0.3 eV that corresponding to pyridinic N (N1), pyrrolic N (N2), and graphitic N (N3), respectively. Analysis of the N_{1s} peaks provides the relative atomic ratios of each type of N species, as shown in Figure 1c, and the resulting schematic model of these N species in carbon backbone is shown in Figure 1d. The pyridinic N atom is located at the edges of the graphitic carbon

layer by substituting a carbon atom on the C_6 ring,[29] which contributes one pair of lone electrons and induces basic properties to the carbon surface. Thus, the adsorption ability of the carbons should be improved due to the strong interatomic attraction between the basic pyridinic N and sulfur and polysulfides species. The pyrrolic N is a nitrogen atom on a five-membered ring and contributes two p-electrons to the π system, which may also be favorable for the surface adsorption but its interaction is not strong as that of pyridinic N. The graphitic nitrogen doped inside the graphitic carbon plane bonds with three sp^2 carbon atoms, which is believed to exhibit higher electronegativity (3.04) compared with C (2.55).[30] The graphitic nitrogen will enable more electrons to be introduced into the layers of graphite, improving the electronic conductivity of the carbon.[31] There is no peak associated with nitrogen bonded to oxygen, which would appear at 404−408 eV, suggesting that the oxygen atoms in the NMCs might be all bonded to the carbon atoms. It is worthwhile to note that at the same pyrolysis temperature of 800 °C, the distribution of these N species is almost similar regardless of the M/P ratio, in which the pyridinic N is the dominant form representing around 60%.

The electronic conductivity of the carbon is generally related to its graphitization degree which is determined by the pyrolysis temperature. In addition, substituting nitrogen into carbon framework can also enhance its electronic conductivity because the nitrogen atoms provide additional free electrons for the conduction band as above-discussed. In this work, the powder electrical resistivities of the NMCs were measured using a four-contact method under the pressure of 4 MPa at room temperature. As listed in Table 1, nitrogen doping could significantly decrease the electrical resistivity, from 12.7 Ω to 2.3 Ω cm by only doping 4.2 wt % nitrogen. Increasing the nitrogen content to 8.1 wt % could slightly increase the electrical resistivity to 6.4 Ω cm, but still on a competitive level. While the nitrogen content is 11.9 wt %, however, the electrical resistivity is remarkably increased to 23.6 Ω cm. This should be due to the excessive nitrogen doping, which damages the integrity of the graphitic structure. Apparently, there is an optimum nitrogen content range (4−8 wt %) at which the effect of doping an additional electron prevails over disordering of the graphite structure.

The textural properties of the NMCs were assessed by N_2 sorption, as shown in Figure 2. The NMCs exhibit very similar isotherm type between type II and IV following the IUPAC classification, indicating that the NMCs are typically mesoporous carbon materials. Due to the identical replication of the colloidal silica nanoparticles, the porosity of these samples is very similar. Their BJH pore size distributions are mostly centered at 10−20 nm and their BET surface areas are quite close to 750 m^2 g^{-1} (Table 1). This could thus minimize the influence of the porosity, which could prompt us to focus on the nitrogen doping on the performance of the resulting NMC/S cathodes.

Characterization of the NMC/S Composites. The elemental sulfur was infiltrated into the mesopores of the NMCs by a classical melt-diffusion method.[25] The content of sulfur in the NMC/S composites could be controlled by the design of the weight composition of sulfur and carbon. As shown in Figure 3, thermogravimetric analysis (TGA) of all composites in nitrogen flow show a weight loss of approximately 60 wt % between 200 and 450 °C, which corresponds to the evaporation of sulfur in the composite
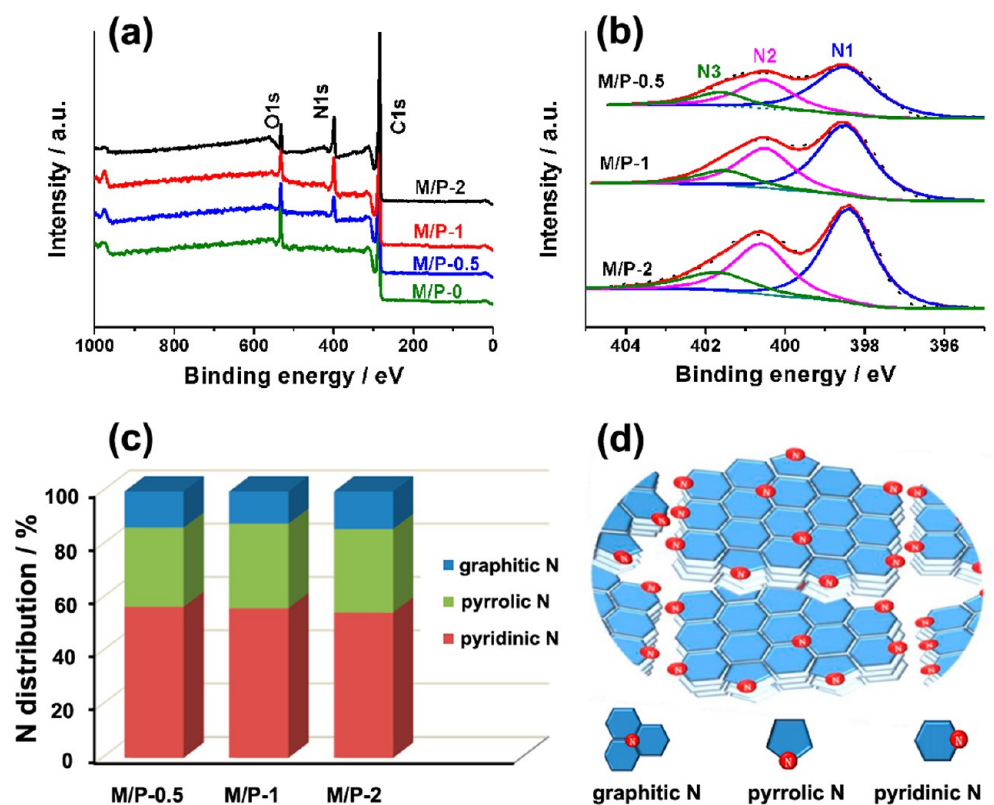
Figure 1. (a) XPS survey and (b) high-resolution N_{1s} spectra of the NMCs with different M/P ratios. (c) Distribution of three nitrogen species (pyridinic N, pyrrolic N, and graphitic N) in the NMCs. (d) Schematic model of three nitrogen species and possible distribution in carbon framework of the NMCs.
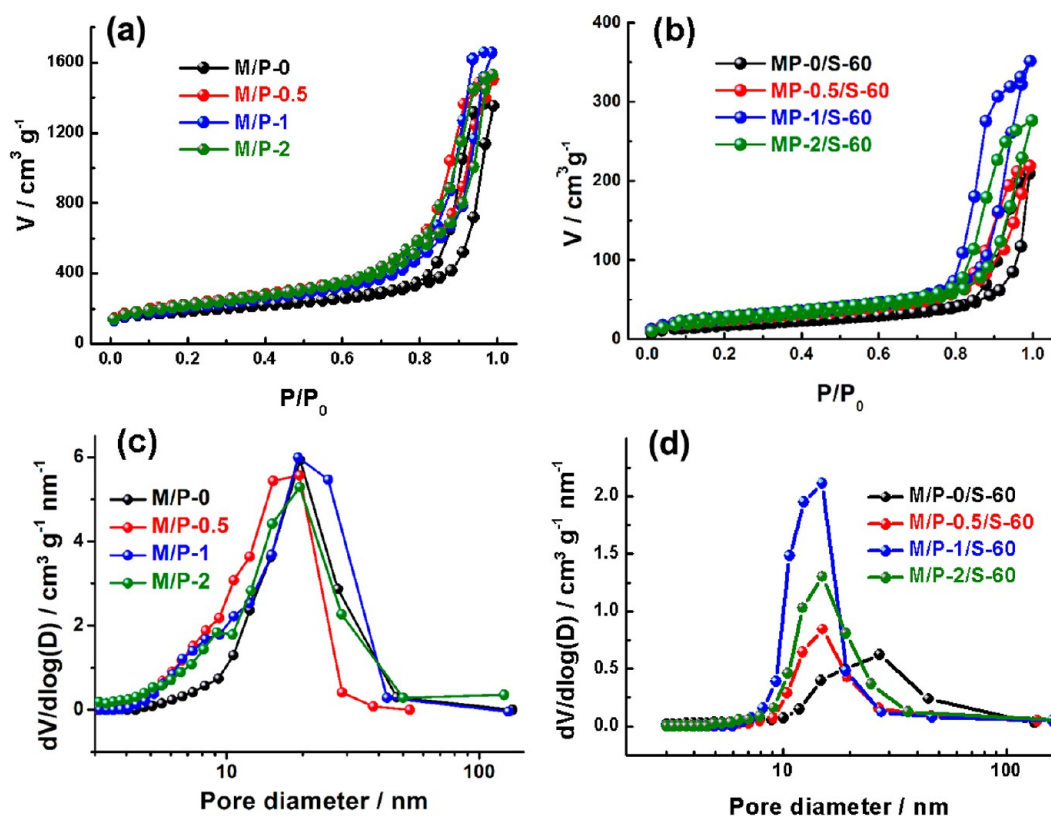
Figure 2. N_2 adsorption−desorption isotherms of the NMCs with different M/P ratios before (a) and after 60 wt % sulfur loading (b). BJH pore size distributions of the NMCs with different M/P ratios before (c) and after 60 wt % sulfur loading (d).
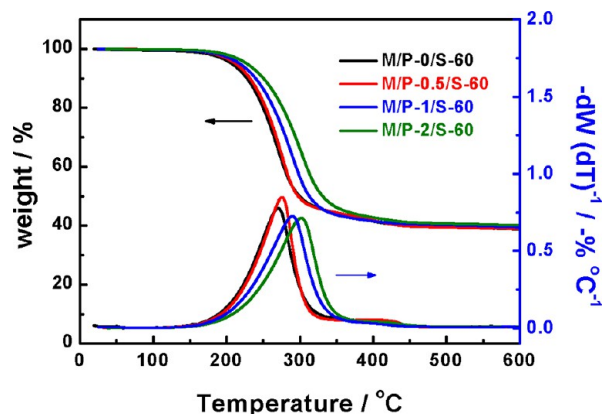
Figure 3. TGA and DTG curves of the 60 wt % sulfur-loaded composites based on the NMCs with different nitrogen contents.

materials. Moreover, compared with nitrogen-free M/P-0/S composites, the sulfur component in the M/P-1 and M/P-2 composites evaporates at a significantly elevated temperature. This might be due to the strong interaction of the basic nitrogen-rich carbon surface and sulfur, responding to a good immobilization capability of the nitrogen-rich carbon surface.

After the impregnation of sulfur, the porosity exhibited the expected decrease as a result of the occupation of a large amount of sulfur into the mesopores. As shown in Figure 2b, at the same sulfur loading of 60 wt %, the M/P-1 with slightly larger pore volume shows a little advantage in terms of sulfur encapsulation, retaining higher mesoporous channels. Still, the other NMC/S composites maintain considerable porosity, allowing the electrolyte and Li ions to penetrate the inner

structure. The structural parameters of the composites are summarized in Supporting Information Table S3. Typically, the composites exhibit a high special area of 65−99 m^2/g and pore volume of 0.3−0.5 cm^3/g.

The sulfur was found to be dispersed in the interconnected spherical mesopores of the NMCs, as revealed by SEM images (Figure 4) before and after the sulfur impregnation. No obvious sulfur agglomerations are observed on the surface of carbon particles (Figure 4d and e). Elemental X-ray mapping (Figure 4g) shows a homogeneous distribution of sulfur within the carbon matrix. These observations confirm that sulfur diffuses into the mesopores of the carbon during the heat-treatment process.

Electrochemical Performance of the NMC/S Composites. The electrochemical performances of all NMC/S composites were evaluated by cyclic voltammetry (CV), galvanostatic charge−discharge testing, and electrochemical impedance spectroscopy (EIS). The CV of the NMC/S composites with 60 wt % sulfur scanned at 0.2 mV s^{-1} are shown in Figure 5a. Two well-defined reduction peaks for all the composites exist distinctly, which are centered at 2.32 and 2.01 V corresponding to the conversion of high-order lithium polysulfides (e.g., Li_2S_8) to low-order lithium polysulfides (Li_2S_x, $4 \leq x < 8$) and lithium polysulfides to solid-state Li_2S_2/Li_2S, respectively.[32] Only one broad oxidation peak is observed, suggesting the transformation of all the polysulfides into the intermediates, which is believed to be S_8^{2-} with the most facile oxidation kinetics. Except for the intensity difference of these peaks between these NMC/S composites, the sulfur reduction onset potential is almost same. In contrast to the conclusion of Sun et al.,[23] our results suggest that nitrogen-doped carbon has
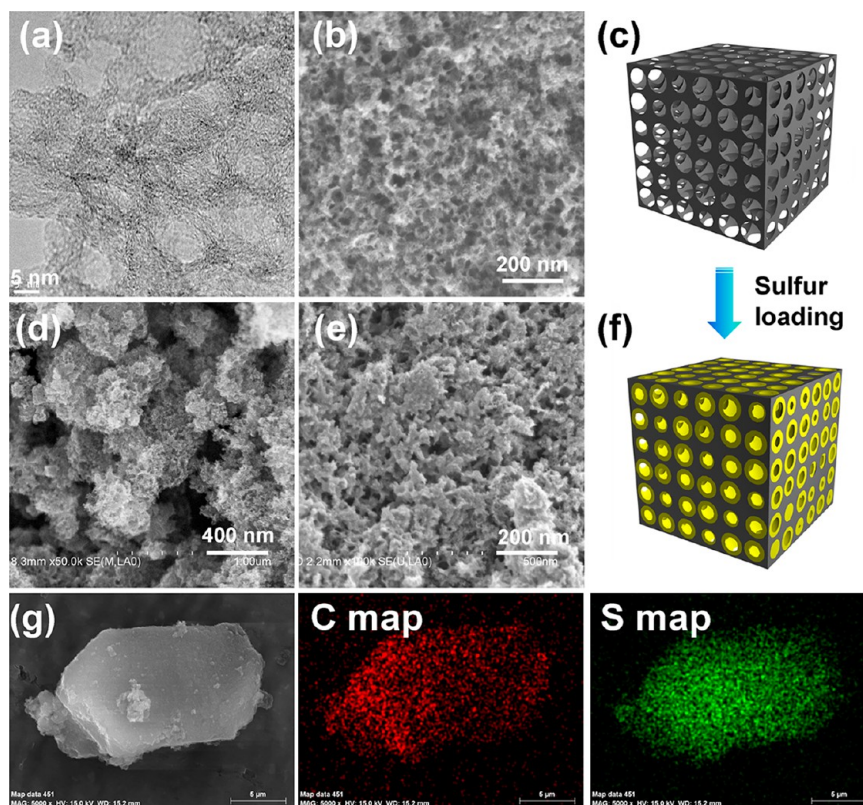
Figure 4. TEM image (a) and SEM image (b) of M/P-1. SEM images of M/P-1/S-60 (d, e). Schematic model of the NMCs (c) and the NMC/S composites (f). SEM mapping of M/P-1/S-60 (g).
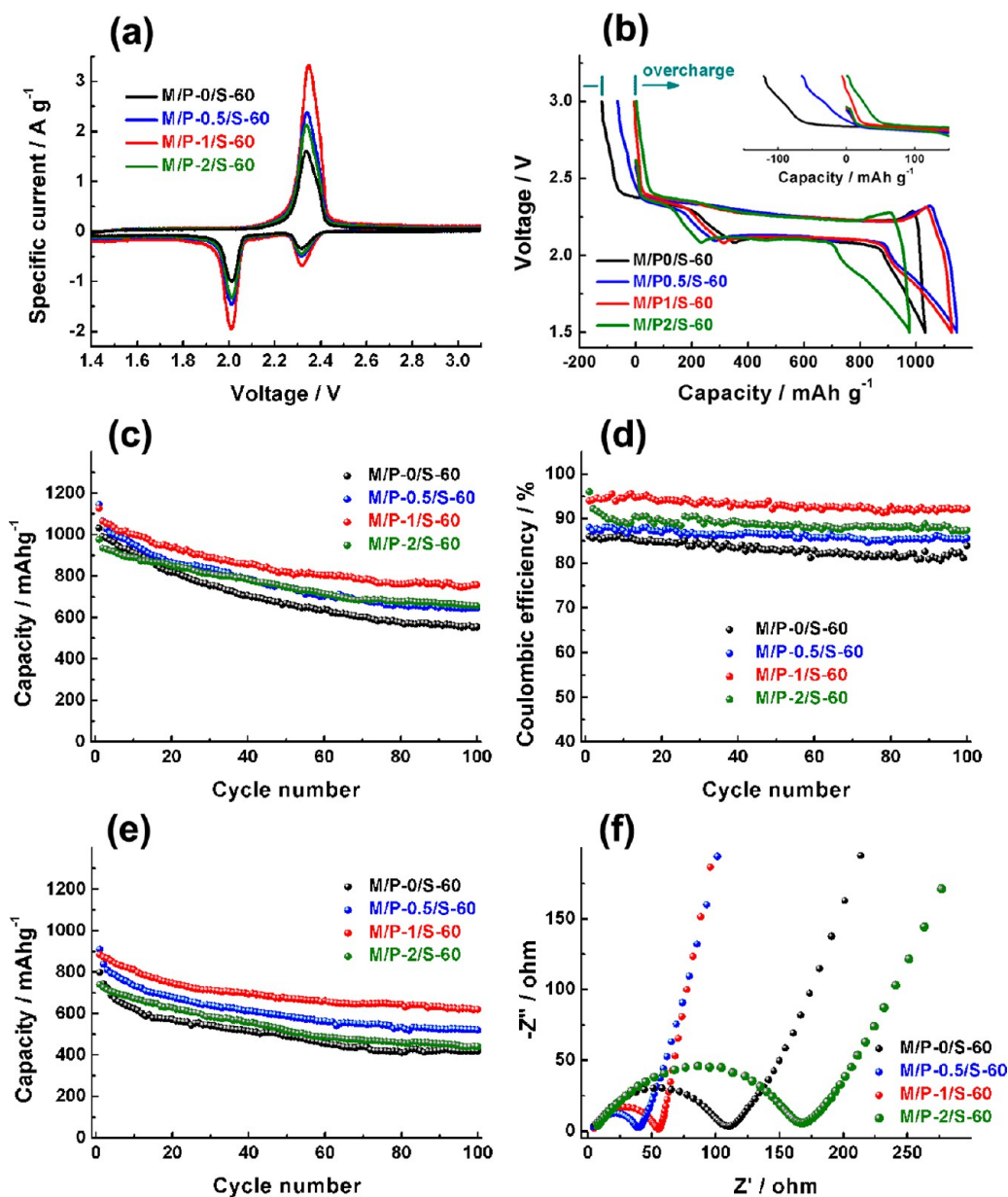
Figure 5. Electrochemical behaviors of the NMC/S-60 based on the NMCs with different nitrogen contents: cyclic voltammograms at 0.2 mV s^{-1} (a); initial charge–discharge curves (b), cycle stability (c), and Coulombic efficiency (d) at 0.2 C. Cycle stability at 1 C (e). EIS before first cycle (f). (b inset) Overcharge capacities of the NMC/S-60 based on the NMCs with different nitrogen contents.

no catalytic activity toward sulfur reduction or nitrogen atoms do not participate in the charge–discharge process of the Li/S battery.

The first discharge and charge profiles of the NMC/S composites with 60 wt % sulfur are shown in Figure 5b. Two plateaus, corresponding to the formation of long-chain polysulfides (Li_2S_x, $4 \leq x \leq 8$) at 2.3 V and short-chain Li_2S_2 and Li_2S at 2.1 V, are observed for all samples in the discharge process, which agree well with two apparent reduction peaks in CV. The M/P-0/S-60 exhibits an obvious overcharge capacity of ca. 120 mA h g^{-1}, which is a typical feature of the polysulfide shuttling phenomenon.[33] This implies that only encapsulation of mesoporous carbon cannot entirely prevent the shuttle phenomenon. Interesting, nitrogen doping could apparently decrease the overcharge capacity. When the nitrogen content in the NMCs is up to 8 wt % (M/P-1 and M/P-2), the overcharge capacity even disappears. Therefore, the basic nitrogen atoms

should serve as immobilizers to anchor polysulfide anions and retard their diffusion.

Figure 5c compares the cycle performance of the composites at a rate of 0.2 C. The M/P-0/S-60 shows an impressive discharge capacity of 1031 mA h g^{-1} (based on the mass of sulfur) in the first cycle, which fades to 555 mA h g^{-1} after 100 cycles. The nitrogen doping could assist mesoporous carbon to improve the sulfur utilization as well as the cycling life in a large degree. When nitrogen content is increased to 8.4 wt %, the M/P-1/S-60 composites exhibit a highest initial discharge capacity of 1145 mA h g^{-1} and reversible capacity after 100 cycles of 758 mA h g^{-1}, as well with a highest Coulombic efficiency of 95% (Figure 5d). The enhanced cycling performance can be attributed to the excellent confining effect of polysulfides of M/P-1/S-60 cathode, which maintain the structural integrity of the composites during the long-term cycling as observed by SEM images (Supporting Information Figure S2). At a higher

current rate of 1 C (Figure 5e), the M/P-1/S-60 composites still deliver a discharge capacity of 620 mA h g^{-1} after 100 cycles. The rate capacity at various current rates up to 5 C are also shown in Supporting Information Figure S3. Such good rate performance is likely due to the facile electronic/ionic transport and improved reaction kinetics in the M/P-1. However, further increasing the nitrogen content to 12 wt %, the composites exhibit a lowest sulfur utilization with a initial discharge capacity of 975 mA h g^{-1} and reversible capacity of 655 mA h g^{-1}, much lower than the values for M/P-1. This is apparently due to the significant deterioration of electronic conductivity caused by the excessive nitrogen doping. EIS results could very confirm this point as shown in Figure 5f. The semicircle diameters in the high frequency region of Nyquist plots reveal that the charge-transfer kinetics are slowest in M/P-2/S-60 composites, in good agreement with the results of the powder electrical resistances (Table 1). Taking these results together, the nitrogen doping could assist the mesoporous carbon to suppress the diffusion of polysulfide species into the electrolyte via a enhanced interface adsorption. However, the total electrochemical performance relies on a synergistic effect between the nitrogen content and the electron conductivity of the carbon. Here a optimal nitrogen content (e.g., 8.4 wt %) is recommended for the carbon host.

The M/P-1/S cathodes with different sulfur loadings were also prepared. Their pore structural characteristics are shown in Supporting Information Figure S4. Due to the developed mesoporous structure of M/P-1, all the composites with different sulfur loadings still contain considerable mesoporous channels, which favor for the access with the electrolyte and buffer the volume expansion of the polysulfides. Thus, the sulfur utilization of the M/P-1/S composites is not strongly affected by increasing the sulfur content from 40 to 60 wt %, as shown in Figure 6. All the composites display a similar initial capacity of about 1140 mA h g^{-1}. After 100 cycles, the M/P-1/S-40 retains a slightly higher reversible capacity of 828 mA h g^{-1}, due to a slightly higher conductivity of the electrode favorable for faster charge-transfer kinetics (see Supporting Information Figure S5).

Undoubtedly, moderate nitrogen doping level is a prerequisite for mesoporous carbons to immobilize sulfur for the enhanced Li–S batteries. However, the capacity fading with cycling is still an intrinsic problem because some lithium polysulfides formed on the carbon external surface could inevitably dissolve into the liquid electrolyte. On the basis of the nitrogen-rich mesoporous carbon encapsulation, here we further employed a PPy/PEG hybrid polymer coating to suppress the polysulfide shuttle, as illustrated in Figure 7a. It has been established that the polymer coating can play important roles in the sulfur electrodes to improve the sulfur utilization, among which conductive PPy is particularly promising.[34,35] However, one problem for PPy is poor mechanical stability, resulting in easy cracking during long-term cycling.[36] Blending rigid PPy with soft PEG is expected to improve mechanical stability of coating layer without losing electronic conductivity.[37,38] Additionally, mixing PEG into PPy films might also enhance ionically conductivity, as PEG is a good solvent for lithium salts.

Figure 7b shows a typical SEM image of PPy/PEG-coated M/P-1/S-60 composite. It is obvious that the surface looks more smooth compared with the bare M/P-1/S-60 composites in Figure 4e, confirming the surface coating of the M/P-1/S-60 by a polymer layer. The TGA curves (Figure 7c) suggest that
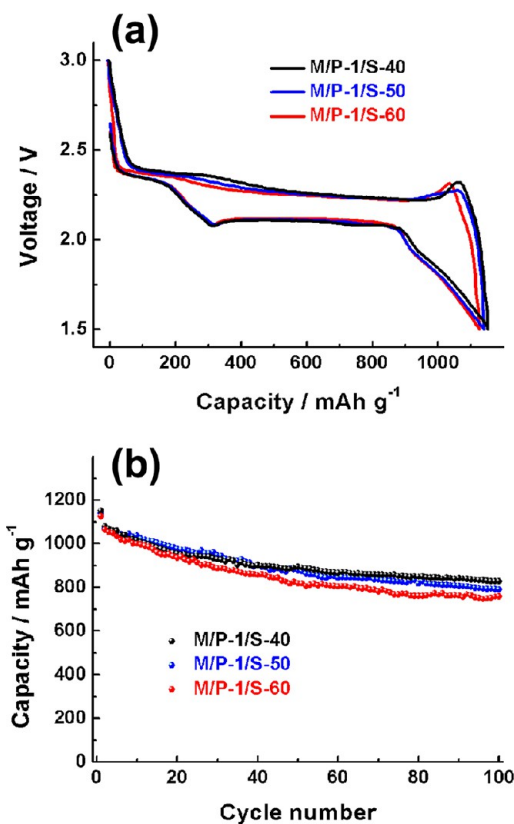

Figure 6. Initial charge–discharge curves (a) and cycle stability of M/P-1/S composites with different sulfur loadings (40, 50, and 60 wt %) at 0.2 C.

the synthesized PPy/PEG-coated M/P-1/S-60 composite is composed of 54.9 wt % sulfur and 9.2 wt % PPy/PEG after considering the mass loss of sulfur and the mass increase from PPy/PEG, which is in good agreement with that obtained by a mass-change calculation. The Raman and XPS results (Supporting Information Figures S6 and S7) could also confirmed the formation of polymer in the synthesized composites. After coating PPy/PEG hybrid polymer, two reduction peaks potentials at 2.32 and 2.01 V are also observed, which is almost the same as bare composites (Supporting Information Figure S8). When cycled at 0.2 C, the PPy/PEG-coated M/P1/S-60 exhibits a much higher reversible capacity of 891 mA h g^{-1} after 100 cycles, which is 17% increase compared with the bare composites (Figure 7d). With the assistance of PPy/PEG coating, the capacity retention rate of M/P-1/S-60 is enhanced from ~67%/100 cycles to ~75%/100 cycles. Such reversible capacity is among the highest values reported for the sulfur cathodes. The PPy/PEG coating is expected to form a stable interface between the liquid electrolyte and lithium polysulfides, allowing fast ion and charge transfer with minimum loss of active materials.

■ CONCLUSIONS

In conclusion, nitrogen-enriched mesoporous carbons with tunable nitrogen content and developed mesoporous structures were prepared by a facile colloid silica nanocasting to house sulfur for Li–S battery. Nitrogen doping could assist mesoporous carbons to suppress the diffusion of polysulfide species via an enhanced surface adsorption, improving the sulfur utilization and cycling performance. In addition, nitrogen
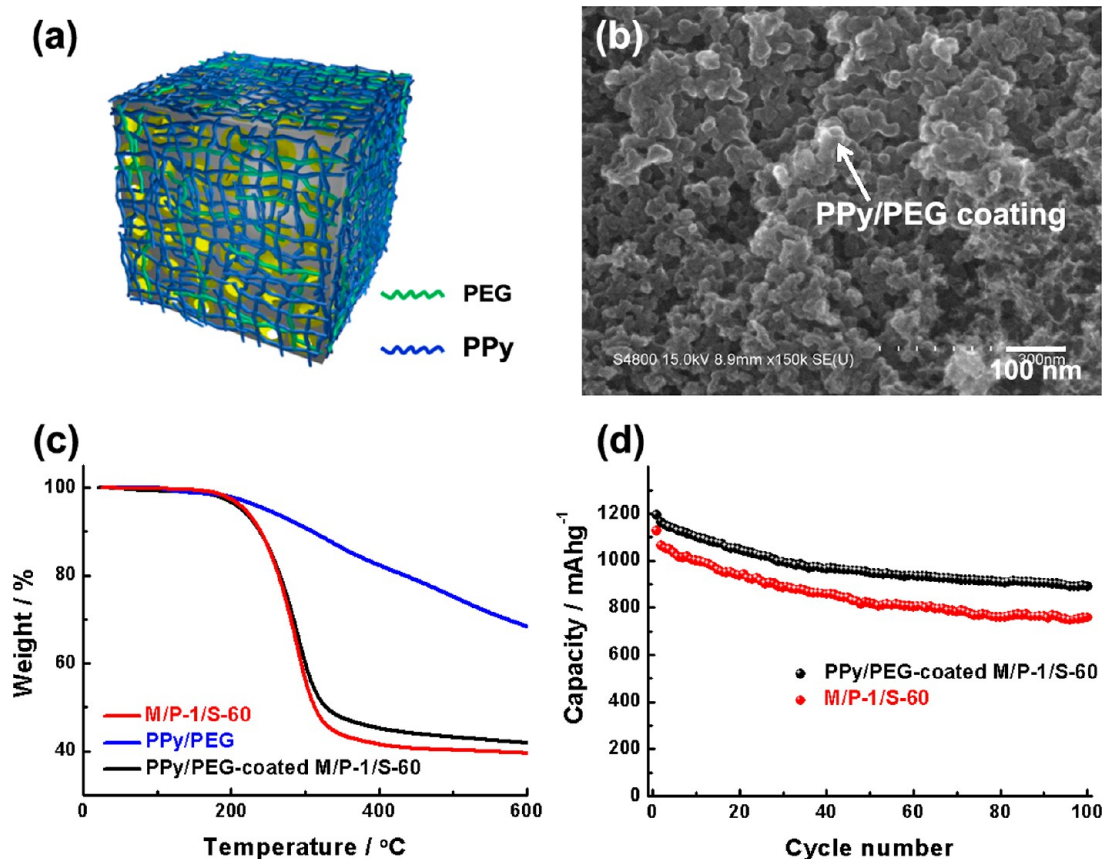
Figure 7. Schematic illustration of the core–shell construction (a) and SEM image (b) of PPy/PEG-coated M/P-1/S-60. TGA curves of M/P-1/S-60, PPy/PEG, and PPy/PEG-coated M/P-1/S-60 composites (c). Cycle stability of PPy/PEG-coated M/P-1/S-60 and M/P-1/S-60 at 0.2 C (d).

doping within an appropriate content range (e.g., 4−8 wt %) could enhance the electronic conductivity of the carbon, offering faster charge-transfer kinetics. In terms of these advantages, the M/P-1/sulfur-60 delivers a very high reversible discharge capacity of 758 mA h g^{-1} at a 0.2 C rate and 620 mA h g^{-1} at a 1 C rate after 100 cycles. Furthermore, the PPy/PEG surface coating could help to further preserve high capacity and maintain high electrochemical stability. A reversible capacity of 891 mA h g^{-1} is obtained after 100 cycles. This work clearly demonstrates that surface chemistry and surface modification of the carbon host play positive roles on the sulfur cathodes for Li−S batteries. These results might also provide some valuable hints for many other energy-storage devices where mesoporous structures are adopted.

■ ASSOCIATED CONTENT

Ⓢ Supporting Information

Elemental analysis and XPS results of the NMCs with different M/P ratios; N$_2$ sorption results of the C/S composites based on NMCs with different M/P ratios; SEM images of MP-0/S-60 and MP-1/S-60 cathodes before first cycle and after 20th cycle; rate capacity of NMC/S-60 cathodes based on the NMCs with different nitrogen contents; EIS before first cycle of the M/P-1/sulfur cathodes with different sulfur loadings; Raman spectra, XPS spectra, and typical cyclic voltammograms at 0.2 mV s^{-1} of MP-1/S-60 and PPy/PEG-coated MP-1/S-60. This material is available free of charge via the Internet at http://pubs.acs.org.

■ AUTHOR INFORMATION

Corresponding Author

*Tel.: +86 21 64252924. Fax: +86 21 64252914. E-mail: longdh@mail.ecust.edu.cn.

Notes

The authors declare no competing financial interest.

■ REFERENCES

(1) Ji, X.; Nazar, L. F. *J. Mater. Chem.* **2010**, *20*, 9821−9826.
(2) Choi, N. S.; Chen, Z.; Freunberger, S. A.; Ji, X.; Sun, Y. K.; Amine, K.; Yushin, G.; Nazar, L. F.; Cho, J.; Bruce, P. G. *Angew. Chem., Int. Ed.* **2012**, *51*, 9994−10024.
(3) Akridge, J. R.; Mikhaylik, Y. V.; White, N. *Solid State Ionics* **2004**, *175*, 243−245.
(4) Ellis, B. L.; Lee, K. T.; Nazar, L. F. *Chem. Mater.* **2010**, *22*, 691−714.
(5) Bruce, P. G.; Freunberger, S. A.; Hardwick, L. J.; Tarascon, J. M. *Nat. Mater.* **2012**, *11*, 19−29.
(6) Zheng, G.; Yang, Y.; Cha, J. J.; Hong, S. S.; Cui, Y. *Nano Lett.* **2011**, *11*, 4462−4467.
(7) Nelson, J.; Misra, S.; Yang, Y.; Jackson, A.; Liu, Y.; Wang, H.; Dai, H.; Andrews, J. C.; Cui, Y.; Toney, M. F. *J. Am. Chem. Soc.* **2012**, *134*, 6337−6343.
(8) Zhang, B.; Lai, C.; Zhou, Z.; Gao, X. P. *Electrochim. Acta* **2009**, *54*, 3708−3713.

(9) Chen, J.; Jia, X.; She, Q.; Wang, C.; Zhang, Q.; Zheng, M.; Dong, Q. *Electrochim. Acta* **2010**, *55*, 8062−8066.

(10) Ji, X.; Lee, K. T.; Nazar, L. F. *Nat. Mater.* **2009**, *8*, 500−506.

(11) Zhang, L.; Ji, L.; Glans, P. A.; Zhang, Y.; Zhu, J.; Guo, J. *Phys. Chem. Chem. Phys.* **2012**, *14*, 13670−13675.

(12) Zhang, B.; Qin, X.; Li, G. R.; Gao, X. P. *Energy Environ. Sci.* **2010**, *3*, 1531−1537.

(13) Wei, S.; Zhang, H.; Huang, Y.; Wang, W.; Xia, Y.; Yu, Z. *Energy Environ. Sci.* **2011**, *4*, 736−740.

(14) Liang, C.; Dudney, N. J.; Howe, J. Y. *Chem. Mater.* **2009**, *21*, 4724−4730.

(15) Jayaprakash, N.; Shen, J.; Moganty, S. S.; Corona, A.; Archer, L. A. *Angew. Chem., Int. Ed.* **2011**, *50*, 5904−5908.

(16) Ji, L.; Rao, M.; Zheng, H.; Zhang, L.; Li, Y.; Duan, W.; Guo, J.; Cairns, E. J.; Zhang, Y. *J. Am. Chem. Soc.* **2011**, *133*, 18522−18525.

(17) Qie, L.; Chen, W.; Wang, Z.; Shao, Q.; Li, X.; Yuan, L.; Hu, X.; Zhang, W.; Huang, Y. *Adv. Mater.* **2012**, *24*, 2047−2050.

(18) Wu, Y.; Fang, S.; Jiang, Y. *J. Mater. Chem.* **1998**, *8*, 2223−2227.

(19) Wu, Y.; Fang, S.; Jiang, Y. Y.; Holze, R. *J. Power Sources* **2002**, *108*, 245−249.

(20) Rodríguez, E.; Camean, I.; Garcia, R.; Garcia, A. B. *Electrochim. Acta* **2011**, *56*, 5090−5094.

(21) Jin, H.; Zhang, H.; Zhong, H.; Zhang, J. *Energy Environ. Sci.* **2011**, *4*, 3389−3394.

(22) Yang, X.; Wu, D.; Chen, X.; Fu, R. *J. Phys. Chem. C* **2010**, *114*, 8581−8586.

(23) Sun, X.; Wang, X.; Mayes, R. T.; Dai, S. *ChemSusChem* **2012**, *5*, 2079−2085.

(24) Long, D.; Chen, Q.; Qiao, W.; Zhan, L.; Liang, X.; Ling, L. *Chem. Commun.* **2009**, *26*, 3898−3900.

(25) Wang, J. T.; Chen, Q. J.; Liu, X. J.; Qiao, W. M.; Long, D. H.; Ling, L. C. *Mater. Chem. Phys.* **2011**, *129*, 1035−1041.

(26) He, G.; Ji, X.; Nazar, L. F. *Energy Environ. Sci.* **2011**, *4*, 2878−2883.

(27) Choi, Y. S.; Joo, S. H.; Lee, S. A.; You, D. J.; Kim, H.; Pak, C.; Chang, H.; Seung, D. *Macromolecules* **2006**, *39*, 3275−3282.

(28) Fedorková, A.; Oriňáková, R.; Oriňák, A.; Wiemhöfer, H.; Kaniansky, D.; Winter, M. *J. Solid State Electrochem.* **2010**, *14*, 2173−2178.

(29) Jurcakova, D. H.; Seredych, M.; Lu, G.; Bandosz, T. J. *Adv. Funct. Mater.* **2009**, *19*, 438−447.

(30) Yang, Z.; Yao, Z.; Li, G.; Fang, G.; Nie, H.; Liu, Z.; Zhou, X.; Chen, X.; Huang, S. *ACS Nano* **2012**, *6*, 205−211.

(31) Seredych, M.; Hulicova-Jurcakova, D.; Lu, G. Q.; Bandosz, T. J. *Carbon* **2008**, *46*, 1475−1488.

(32) Li, X.; Cao, Y.; Qi, W.; Saraf, L. V.; Xiao, J.; Nie, Z.; Mietek, J.; Zhang, J.; Schwenzer, B.; Liu, J. *J. Mater. Chem.* **2011**, *21*, 16603−16610.

(33) Schuster, J.; He, G.; Mandlmeier, B.; Yim, T.; Lee, K. T.; Bein, T.; Nazar, L. F. *Angew. Chem., Int. Ed.* **2012**, *51*, 3591−3595.

(34) Liang, X.; Wen, Z.; Liu, Y.; Zhang, H.; Jin, J.; Wu, M.; Wu, X. *J. Power Sources* **2012**, *206*, 409−413.

(35) Fu, Y.; Manthiram, A. *J. Phys. Chem. C* **2012**, *116*, 8910−8915.

(36) Yang, Y.; Yu, G.; Cha, J. J; Wu, H.; Vosgueritchian, M.; Yao, Y.; Bao, Z.; Cui, Y. *ACS Nano* **2011**, *5*, 9187−9193.

(37) Kang, H. C.; Geckeler, K. E. *Polymer* **2000**, *41*, 6931−6934.

(38) Fedorková, A.; Nacher-Alejos, A.; Gómez-Romero, P.; Orinákovác, R.; Kaniansky, D. *Electrochim. Acta* **2010**, *55*, 943−947.